INTERNATIONAL JOURNAL OF AUTOMOTIVE AND MECHANICAL ENGINEERING
ISSN: 2229-8649 e-ISSN: 2180-1606
VOLUME 22, ISSUE 4, 2025, 13043 - 13057
DOI: https://doi.org/10.15282/ijame.22.4.2025.16.0993

RESEARCH ARTICLE

Design and Finite Element Modeling of a Robust MEMS Capacitive Accelerometer for Automotive Airbag Applications

Mahdi Al Quran[1*], Ahmad Al-Sheyyab[2], Mutaz Al-Otain[3], Wesam AlJaiuossi[4]

[1]Department of Mechanical Engineering, Faculty of Engineering, The Hashemite University, P.O. Box 330127, Zarqa, 13133, Jordan
[2]Aeronautical Engineering Department, Jordan University of Science and Technology, Irbid, 22110, Jordan
[3]Jordan Design and Development Bureau (JODDB), P.O Box 6384, Amman 11118, Jordan
[4]National Electric Power Company (NEPCO), Zahran St 275, Amman, Jordan

ABSTRACT – This study presents a robust single-axis Micro-Electro-Mechanical Systems (MEMS) capacitive accelerometer designed for airbag applications. Most of the designs presented in the literature have complicated designs, lower sensitivity, and large device areas. Moreover, most literature studies design accelerometers to measure acceleration up to 10g. In this connection, this research work presents a simple, compact, and lightweight accelerometer capable of operating in a wide range of accelerations from -50g to 50g. Moreover, the present design introduces small holes over the proof mass to reduce weight, and these etch holes facilitate the release of the proof mass during fabrication. To analyze the performance of the proposed design, Finite Element Modeling (FEM) was performed to evaluate the resonant frequency, mode shapes, stress, and deformation under applied acceleration/deceleration, as well as during a car crushing test. Study results found that the proposed accelerometer has a dominant resonant frequency of 8.3 kHz. This result was confirmed through complementary analytical calculations, demonstrating a strong agreement between experimental and theoretical findings. To evaluate the durability and stability of the accelerometer, stress analysis was conducted over the applied range of acceleration values. It was found that the stresses produced within the designed accelerometer are significantly below the material's yield strength. The maximum ΣVM (Von-Mises stress) and τmax (maximum shear stress) experienced by the proposed accelerometer are approximately 3.05 MPa and 1.64 MPa, respectively. Consequently, the proposed accelerometer demonstrated safe operation within the acceleration envelope of -100g to 100g without incurring mechanical failure. The accelerometer exhibits exceptional sensitivity, achieving a displacement sensitivity of 0.00363 µm/g and a capacitive sensitivity of approximately 0.000339 pF/g. Moreover, the shock test and the effect of environmental conditions, i.e., temperature, are also carried out to understand the designed accelerometer's behavior in real-world applications. It was found that the stresses produced under impact conditions and at elevated temperature were lower than the yield strength of the material, therefore, the designed accelerometer will remain safe.

ARTICLE HISTORY
Received : 10th Apr. 2025
Revised : 09th Oct. 2025
Accepted : 04th Nov. 2025
Published : 19th Nov. 2025

KEYWORDS
MEMS
Capacitive accelerometer
Automotive airbag
Finite element analysis

1. INTRODUCTION

Advancements in microelectromechanical systems (MEMS) technology have facilitated the large-scale production of compact and affordable accelerometers. MEMS-based accelerometers are now extensively utilized across various industries, including consumer electronics, automotive systems, and seismic data acquisition [1-3]. Moreover, MEMS accelerometers are now widely used in various technological fields, including wearable technology [4, 5] and structural health monitoring systems [6, 7]. The accelerometer is designed to achieve several objectives, including a minimal footprint, low nonlinearity, and high sensitivity [8]. The primary classifications of accelerometers encompass several distinct types, including those based on piezoresistive, capacitive, optical, thermal, and tunneling principles, due to their distinct transduction mechanisms. Nevertheless, capacitive accelerometers provide substantial advantages over alternative accelerometer technologies due to their superior accuracy, uncomplicated fabrication, reduced thermal sensitivity, low power consumption, and enhanced integration capabilities [9].

The accelerometer consists of an elastic beam, serving as the potential energy storage element, and a proof mass, which stores kinetic energy. These components together create a vibrating system with one degree of freedom. The movable proof mass is coupled to the comb structure in order to achieve a significant capacitance change. In general, the movement of the comb structure can be quantified by measuring either detecting changes in the overlapping conductive area (common in area change accelerometers) or sensing variations in the gap between adjacent finger structures (typical of gap closure accelerometers) [10, 11]. The capacitance changes linearly with movement when using the area change sense technique, however, the sensitivity is limited. On the other hand, due to its high sensitivity, the gap change sense technique is frequently employed.

***CORRESPONDING AUTHOR | M. Al Quran** | ✉ mahdij@hu.edu.jo

The design objectives of the accelerometer include a small footprint, large bandwidth, minimal nonlinearity, and high sensitivity. Additionally, large numbers of fingers, low-stiffness springs, and a short finger gap are all beneficial for achieving high sensitivity. However, incorporating more comb fingers into the design demands a correspondingly scaled-up proof mass, resulting in a larger footprint. On the other hand, the low-stiffness springs limit the bandwidth. Hence, designing a sensor with both high sensitivity and a wide bandwidth is a challenging task. This trade-off can be simplified by using a very small finger gap. For instance, Chaudhuri [1] obtained a broad 3dB bandwidth of 10 kHz and enhanced sensitivity with a gap of 500 nm.

Ramakrishnan et al. [12] designed a single-axis MEMS capacitive accelerometer for automotive airbag deployment applications. Structural and modal analyses were conducted to evaluate the resonance frequencies and internal stress distribution of the device. The optimized accelerometer possessed a compact device footprint of 4 mm^2 and demonstrated a displacement sensitivity of 0.653 μm/g, ensuring stable and reliable operation under acceleration levels of up to 15 g. Koochaksaraie et al. [13] designed a dual-spring MEMS capacitive accelerometer for a high acceleration range from 12 to 75g. The proposed accelerometer has a device area of 2.72 mm^2, a mechanical sensitivity of 0.0092μm/g and a resonant frequency of 1774 Hz. Moreover, the various commercial accelerometers from STMicroelectronics and Bosch were carefully studied to design a MEMS capacitive accelerometer for real-world automotive airbag applications. The accelerometers designed by STMicroelectronics and Bosch have an acceleration range of ±8 to ±120g for automotive airbag applications; however, the device area and weight of these accelerometers are significantly higher compared to the proposed accelerometer design. Moreover, the operating temperature range of these accelerometers is typically between -50 °C and 140 °C. In contrast, the proposed accelerometer design is safe under various environmental conditions, including temperatures of up to 150 °C.

A comprehensive literature review indicates that the design, analysis, and manufacturing of MEMS accelerometers remain a dynamic research field due to their widespread applications in various sectors, including the automotive industry, robotics, consumer electronics, navigation, healthcare, and seismic surveys [14-18]. Besides, more Contemporary research has focused on improving the accuracy of these devices [19-22]. There has been minimal research conducted on the development and evaluation of MEMS accelerometer technology specifically for automotive airbag applications. The major challenges of these studies are the complicated design, low range of acceleration force, large size, and lower mechanical as well as capacitive sensitivity [12]. Recently, several studies analyzed the system-level operation of MEMS accelerometers for automotive applications. [23-27]. Moreover, Modern optimization algorithms have been deployed to enhance the airbag design in automotive applications[28-30]. In addition, numerous studies examined the thermal effects [31-33], shock and impact [34-37], and other considerations [38-41].

To overcome the aforementioned challenges, this study presents the design and analysis of a simple, lightweight, and easy-to-manufacture and maintain MEMS capacitive accelerometer. The proposed accelerometer exhibits enhanced sensitivity, a compact form factor, and excellent structural resilience. Once the design parameters are finalized, a three-dimensional Computer-Aided Design (CAD) model of the MEMS accelerometer was developed and subsequently analyzed to determine the resonance frequency. An additional distinctive feature of the proposed design is the utilization of etch holes in the proof mass to simplify the release process of the thin structure during manufacturing. Moreover, the results for the resonance frequency are calculated analytically and using simulation. FEM is also performed to determine the deformation, stresses, mechanical sensitivity, and capacitive sensitivity of the designed accelerometer.

2. METHODOLOGY

2.1 MEMS Accelerometer: Structural and Operational Fundamentals

The MEMS structure illustrated in Figure 1 is that of a single-axis, in-plane accelerometer, featuring a differential capacitive design with comb finger electrodes. The characteristics of MEMS capacitive accelerometers, including their simple design, ease of manufacturability, and high sensitivity, offer the advantages of a transduction mechanism that is not significantly affected by temperature, exhibits low drift, and demonstrates low noise levels, making them suitable for numerous applications. A differential MEMS capacitive accelerometer is comprised of several parts: anchors, what is termed a 'beam' (realized as a folded spring), the proof mass, and sets of movable and fixed fingers. The comb drive capacitive accelerometer operates on the following basic principle: first, if the accelerometer experiences no external acceleration (a=0), there is no change in capacitance because the distance between the movable and fixed fingers remains constant. The second scenario involves subjecting the accelerometer to an external acceleration. This input acceleration is then imparted to the proof mass, causing the proof mass and its associated movable finger structures to move in response, following the direction of the applied force. Because the fixed fingers remain in place, the spacing between the fingers varies, resulting in a change in capacitance. Acceleration is measured using the change in capacitance in this framework [42-45]. As depicted in the middle and right portions of Figure 2, the second condition is shown.

Under zero-acceleration conditions (a=0) for the MEMS accelerometer, Figure 2 (left) illustrates the movable finger resting in the midpoint between the fixed fingers. In this state, the left and right capacitances (C_2) are equal, representing the rest capacitance (C_0), and are calculated as follows:

$$C = C_0 = \frac{\epsilon_0 A}{d} = \frac{\epsilon_0 N_s L_f t}{d} \quad (1)$$

whereas in Equation (1) ϵ_0 and N_s denote the air permittivity along with the count of sensing fingers, respectively. The movable finger length and the MEMS accelerometer thickness are represented by L_f and t, respectively, whereas d denotes the distance between the movable and fixed fingers. Let us assume a non-zero acceleration is applied to the MEMS accelerometer; the fingers will move to the left or right by a non-zero displacement x, as shown in Figure 2 (left and right). Due to the movement of the fingers, the distance between the fingers on one side becomes d + x, and subsequently, the capacitance at this side becomes C_1. On the other side, the distance will be reduced by x to become d-x, and subsequently, the capacitance becomes C_2. The values of C_1 and C_2 can be determined using equations 2 and 3, respectively [46, 47].

$$C_1 = \frac{\epsilon_0 N_s L_f t}{d + x} \tag{2}$$

$$C_2 = \frac{\epsilon_0 N_s L_f t}{d - x} \tag{3}$$

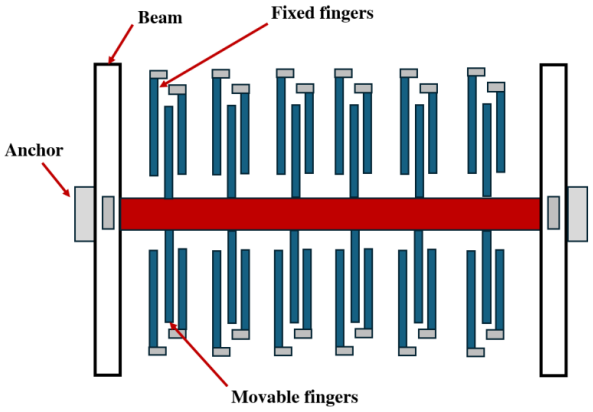

Figure 1. Single-axis MEMS accelerometer structure showing the proof mass, suspension beam, anchors, movable and fixed fingers [7]

To maintain linearity, as one of the key requirements of an effective design, the displacement (x) needs to be considerably less than the spacing (d) between the fingers. Moreover, maintaining the accelerometer's linear response necessitates that the displacement induced by the applied acceleration remains within a 20% tolerance of the inter-finger gap, denoted as 'd'. Simplified forms of the previously mentioned equations 2 and 3 can be expressed as:

$$C_1 = \frac{\epsilon_0 N_s L_f t}{d + x} = \frac{\epsilon_0 N_s L_f t}{d}\left(1 - \frac{x}{d}\right) \tag{4}$$

$$C_2 = \frac{\epsilon_0 N_s L_f t}{d - x} = \frac{\epsilon_0 N_s L_f t}{d}\left(1 + \frac{x}{d}\right) \tag{5}$$

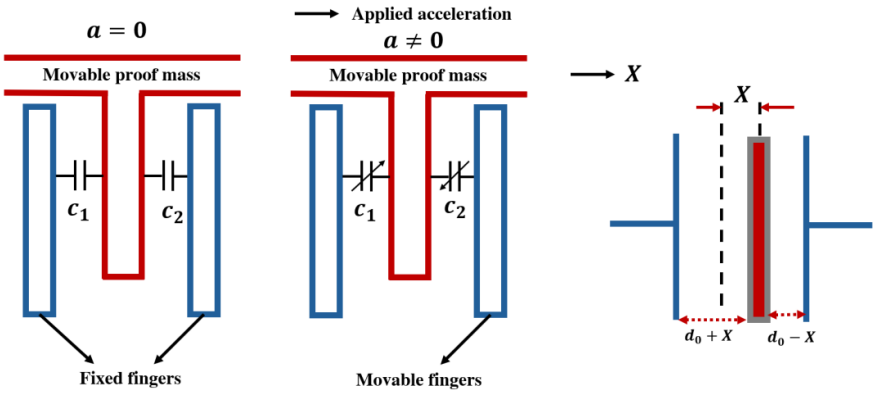

(a) (b) (c)

Figure 2. Illustration of the working principle for a single-axis MEMS accelerometer. (a) Movable finger position at zero acceleration. (b) Movable finger position under non-zero acceleration impacting the proof mass. (c) Displacement of the movable finger resulting from applied acceleration [7]

Thus, when the accelerometer is subjected to a non-zero acceleration, a disparity arises between the capacitances C_1 and C_2. The resulting difference in these capacitances can then be calculated based on the equation provided below:

$$\Delta C = C_1 - C_2 = \frac{\epsilon_0 N_s L_f t}{d}\left(1 - \frac{x}{d}\right) - \frac{\epsilon_0 N_s L_f t}{d}\left(1 + \frac{x}{d}\right) \tag{6}$$

$$\Delta C = 2C_0\left(\frac{x}{d}\right) \tag{7}$$

where C_0 is the static capacitance.

2.2 Dynamic Modelling of MEMS Accelerometer

Vibratory transduction is the fundamental principle underlying the operation of the single-axis MEMS differential capacitive accelerometer. The MEMS accelerometer comprises a single-degree-of-freedom vibrating system in which anchor-fixed beams act as the supporting springs for the proof mass. The elastic beam serves as a spring, storing the potential energy of the system, while kinetic energy storage primarily occurs in the proof mass. Neglecting the aerodynamic drag, the vibration analysis of the accelerometer is conducted by considering it as a single DOF vibrating system, where the proof mass is allowed to move in one direction [7, 45-47] (Figure 3).

When the single DOF vibrating system is subjected to external excitation, then different internal forces are generated inside the system, such as inertial force due to acceleration of mass, spring force due to compression or expansion of spring, and damping force produced as a result of material damping or viscous air damping. Mathematically, the force balance in the x-direction will be written as

$$m\ddot{x} + b\dot{x} + kx = mg \tag{8}$$

In the above equation, m represents the proof mass, b refers to the damping coefficient, and k represents the spring stiffness. Moreover, the displacement of mass is denoted by x, and the external acceleration is represented by $\ddot{x}$. The equivalent spring stiffness of the folded springs is computed by applying the following equation [7, 45-47].

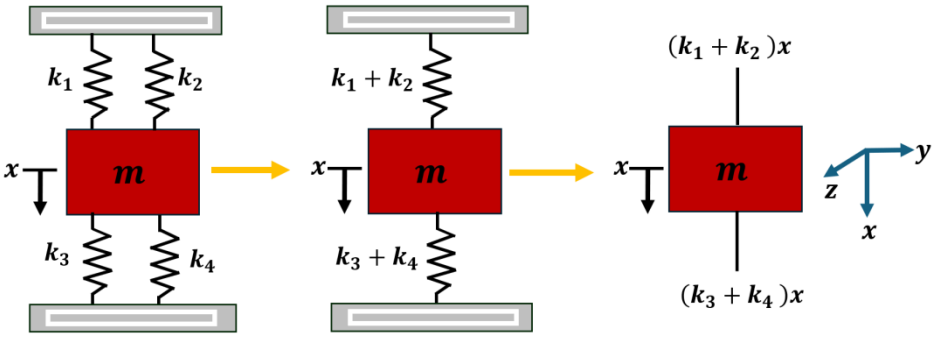

Figure 3. The formulation of a mathematical framework for the vibrational analysis of a 3-axis capacitive MEMS accelerometer [7]

$$K_{eq} = \frac{4EW_b^2 t}{L_b^3} \tag{9}$$

In Equation (9), E and Wb represent the beam material's Young's Modulus along with the beam's width, respectively. Furthermore, t and Lb refer to the thickness and beam folded length, respectively. Once the beam stiffness is computed, the sensing mass of the beam m_s is calculated by applying the following relationship

$$m_s = \rho t\left[W_m L_m + N_f W_f L_f\right] \tag{10}$$

where ρ represents the density of the poly-silicon material. W_m denotes the width of the proof mass in the single-axis MEMS accelerometer. L_m refers to its length. Also, N_f , W_f , and L_f the quantity of movable fingers along with the specific width of each individual finger, and the movable finger length, respectively. To compute the resonant frequency of the specific single-axis MEMS capacitive accelerometer design, the following formula is applied:

$$f_0 = \frac{1}{2\pi}\sqrt{\frac{K_{eq}}{m_s}} \tag{11}$$

In which f_0 is the frequency at resonance for the accelerometer, K_{eq} is the total spring constant, and m_s is the sensing mass. The displacement sensitivity of the single-axis MEMS accelerometer in the sensitive direction s_d can be determined by the following relationship:

$$s_d = \frac{\rho t\left[W_m L_m + N_f W_f L_f\right] L_b^3}{4EtW_b^3} \tag{12}$$

Two primary damping mechanisms affect MEMS structures. Structural damping arises from internal friction within the material [48], while viscous damping results from air interaction at ambient conditions, depending on the fluid

properties and device geometry [49, 50]. Squeeze-film damping occurs when pressure variations develop in the air gap between closely spaced plates. The damping coefficient of a comb-type capacitive accelerometer is given by Equation (13) [51].

$$b=N\mu_{eff} l \left(\frac{t}{d}\right)^3 \tag{13}$$

whereas in the above equation (13), μ_{eff} effective viscosity, l, represents the overlapping length, t denotes device thickness, and d represents the gap between fixed and movable fingers. Two distinct damping components are associated with the gap and anti-gap regions, and their cumulative effect is taken into account in the subsequent analysis.

2.3 CAD Modelling and Meshing of the Accelerometer

To achieve the set objectives of compact design, lightweight, and highly sensitive design, a comb-type single-axis differential capacitive MEMS accelerometer is designed after a thorough literature review regarding the dimensions of the beam, the gap between fingers, and the proof mass dimensions. Table 1 outlines the design specifications for the MEMS accelerometer. The CAD model designed and simulated for the single-axis MEMS capacitive accelerometer excluded fixed fingers. However, it featured four folded springs and a proof mass that included movable fingers. Moreover, the presence of etch holes facilitates the timely release of the proof mass during its fabrication process. The sensor's footprint and fabrication constraints are decreased by its straightforward design, which eliminates the need for intricate wire bonding and electrical isolation. A different approach to this research is to create a MEMS accelerometer using just one lithography stage. This strategy can lower expenses while improving process reliability.

Table 1. Design specification of the accelerometer

Parameter	Value
Width of the beam (W_b)	2µm
Length of the beam (L_b)	250µm
Width of the mass (W_m)	70µm
Length of the mass (L_m)	400µm
Width of the movable finger (W_f)	4µm
Length of the movable finger (L_f)	680 µm
Total number of sensing finger (N_f)	33
Thickness of the device (t)	8µm
Anchor size	20 µm ×20 µm
Outside device area	500 µm × 520µm
Hole diameter	10 µm
Sensing mass (m_s)	1.39 µg
Static capacitance	0.187 pf

Figure 4 (a) illustrates the CAD representation of the differential capacitive MEMS accelerometer design. Once the CAD model is designed, the accelerometer's domain is meshed using the ANSYS Meshing tool, a process that divides the complete, continuous geometry into a finite set of discrete elements. The Cubic mesh elements were used to generate the mesh, and the impact of mesh element size was also analyzed, where the mesh element size was varied from 5µm to 1 µm. Figure 4 (b) and (c) display the meshed model of the differential capacitive MEMS accelerometer. Figure 4 also provides a close-up illustration of the meshed model (b), showing that cubic mesh elements are used. Moreover, further mesh details such as the total number of elements, total number of mesh nodes, and mesh orthogonal quality are shown in Table 2.

(a) (b) (c)

Figure 4. (a) The isometric view of the three-dimensional CAD model of the single-axis MEMS capacitive accelerometer (b) Meshed model of the MEMS capacitive accelerometer (c) Zoomed view of the meshed model showing the type of elements used to generate the mesh

Table 2. Meshing parameters, specifying an element size of 1µm

Domain	Solid
Type of element	Cubic
Quality of orthogonality	0.99383
Element quantity	611160
Node quantity	3022688

The present work considers that the single-axis MEMS differential capacitive accelerometer is made of polysilicon, as numerous studies have utilized this material. Moreover, the mechanical properties of poly-silicon are presented as follows [46]:

- Polysilicon's Young's Modulus (E) =160 GPa
- Polysilicon's density (ρ) =2330 kg/m3
- Polysilicon's Poisson's ratio = 0.22

2.4 Applying Loads and Constraints for Modal Analysis

Elastic structures vibrate under applied loads in the form of special shapes called mode shapes, each of which corresponds to a natural frequency. In the current research, the natural frequencies for the first ten mode shapes are identified through modal analysis. For modal analysis, after the material has been chosen and the meshing procedure has been executed, the most important step in the FEM is to apply constraints and loads according to the problem's physics. Before determining the natural frequencies of the differential MEMS accelerometer, it is necessary to calculate the structural mass and stiffness. Once the design is completed and the material is selected, the parameters will be calculated. The modal analysis doesn't require any external load. The MEMS accelerometer is fixed at its anchors. Additionally, the impact of air and material damping is neglected due to their negligible effect on the resonant frequency. The applied loads and the constraints on the MEMS differential accelerometer are presented in Figure 5.

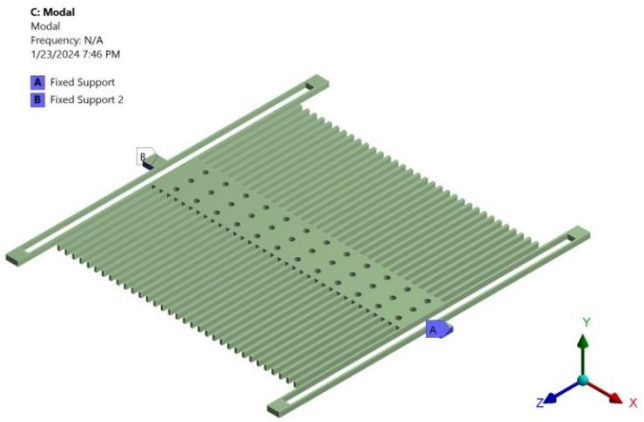

Figure 5. Illustration of the constraints imposed for the accelerometer's modal analysis

2.5 Grid Independence Test

A grid independency test is carried out to evaluate how mesh element dimensions affect the element size on the FEM results at the resonant frequency. For this purpose, different element-size meshes have been generated to obtain a mesh-size-independent solution. The mesh element size ranges from 5 to 0.5 µm, with an insignificant effect on resonant frequency when reduced from 1 µm to 0.5 µm. Moreover, the results of GIT are plotted and presented in Figure 6, where the number of elements is plotted on the x-axis and the resonant frequency on the y-axis. From the graph, a reduction in mesh size is observed to correlate with a decrease in resonant frequency, leading to improved convergence towards the theoretically computed value. Additionally, the effect of grid size on stress and deformation is examined. A reduction in element size from 1.5 µm to 1 µm was implemented for this analysis. It is found that stress and deformation don't show significant variations; therefore, only the results of resonant frequency are presented here.

2.6 Static Structural Analysis

An analysis of the stress and deformation of a single-axis MEMS differential accelerometer is conducted to assess its structural integrity. The stress analysis is performed, in which polysilicon material is selected for fabricating the MEMS accelerometer. Moreover, the same mesh element size is employed in stress analysis. In the case of stress analysis, the MEMS accelerometer was constrained at its anchor points, and acceleration loads of -50g and 50g were applied with an interval of 5g. The study involves analyzing both σ_{VM} (Von-Mises stress) and τmax (maximum shear stress). Details regarding the applied constraints and loads utilized can be found in Figure 7.

3. RESULTS AND DISCUSSION

3.1 Modal analysis

This section presents the modal analysis and stress analysis to design a lightweight, compact and mechanically safe accelerometer. The outcomes of the modal analysis, including resonant frequencies and their corresponding mode shapes, are introduced first. To begin, the proposed accelerometer undergoes modal analysis to determine its resonant frequency. Furthermore, the resonant frequency is also computed analytically according to Equation (2). The numerical simulation results and analytically computed values of resonant frequency are presented in Table 3.

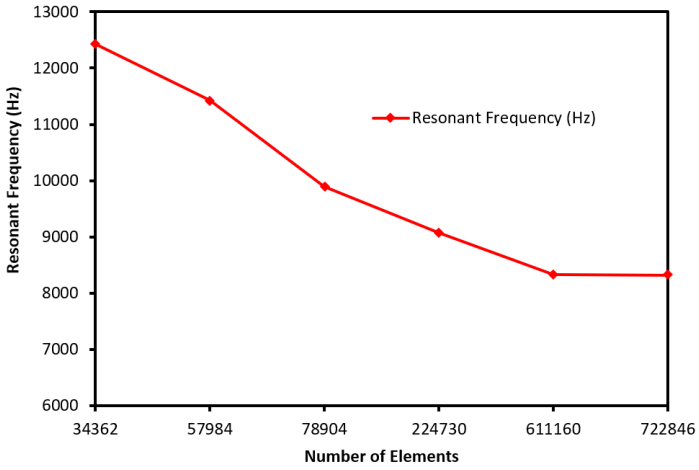

Figure 6. Relationship between resonant frequency and number of elements (i.e, element size)

The comparison of numerical versus analytical values of the resonant frequency reveals that FEM overestimates the resonant frequency; however, the percent error is estimated and found to be quite low. The deviation between analytical and numerical values may be due to the assumption considered in the development of the vibration analysis model, the discretization of the continuous domain into the discrete domain, and the applied constraints.

Three different patterns of motion for the elastic structure, known as mode shapes, are depicted in Figure 8 (a) - (c). The particular mode shape corresponding to the initial resonant frequency is shown in Figure 8 (a). An analysis of this first mode shape indicates that during its resonant state, the single-axis MEMS accelerometer structure vibrates predominantly in the x-direction. Figure 8 illustrates the mode shape corresponding to the y-axis (b), where the accelerometer structure vibrates along the horizontal plane or oscillates along the y-axis. The corresponding frequency is also presented in a contour. Moreover, the random mode shape is presented in Figure 8 (c) along with its corresponding frequency.

Table 3. Comparative Data: Resonant frequencies determined from simulation and analytical computation

Parameter	Analytical value	Simulation value	% Error
Resonant frequency	7123	8332	14%

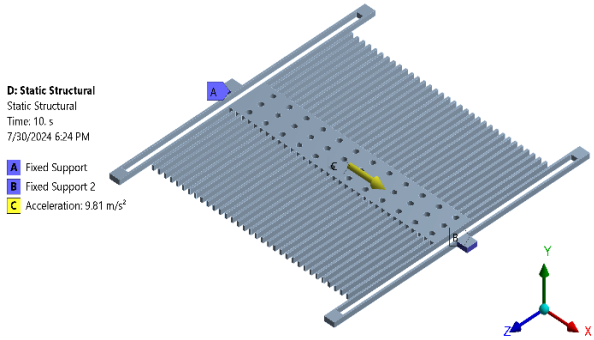

Figure 7. The boundary conditions employed for stress analysis of a single-axis MEMS accelerometer. The fixation of the accelerometer occurred at two anchors, while the acceleration input was aligned with the length of the proof mass

The accelerometer experiences both structural damping and viscous damping during operation. To analyze the impact of damping on the natural frequency of the system, the damping factor is calculated using Equation (13). Moreover, by adding a damping effect, the resonant frequency of the damper decreases the acceleration by approximately 3% as compared to the undamped resonance frequency.

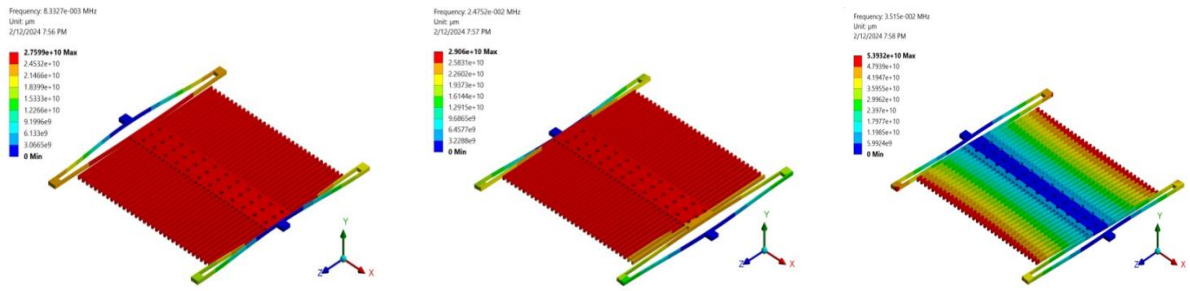

(a) (b) (c)

Figure 8. (a-c) First three consecutive vibration modes of the accelerometer

Table 4. Effect of damping on the resonance frequency

Parameter	Undamped Resonant frequency	Damped Resonant frequency	% decrease in resonance frequency
Resonant frequency	8332	8096	3%

3.2 Stress Analysis

In this section, the results of stresses and deformations are presented and discussed for different values of applied acceleration. The applied acceleration value varies within the range of -50g to 50g with an interval of 5g. The stresses produced within the single-axis differential MEMS accelerometer don't depend on the direction of applied acceleration; therefore, the results of σVM (Von Mises stress) and τmax (maximum shear stress) are presented only for accelerations from 0 to 50g. Figure 9 plots the changes in σ_{VM} (Von-Mises stress) and τmax (maximum shear stress) as a response to the applied acceleration. From the stress analysis results, it is found that both σ_{VM} (Von Mises stress) and τmax (maximum shear stress) exhibit a linear relationship with acceleration. Moreover, the maximum σ_{VM} (Von-Mises stress) and τmax (maximum shear stress) are approximately 3.05 MPa and 1.64 MPa, respectively, which are considerably below the material's yield strength. Hence, the proposed accelerometer will remain safe at the applied acceleration value of 50g. In addition, the designed accelerometer was also tested at an applied acceleration of 100g, and it was found that the stresses were within the yield limit. Thus, the designed accelerometer is able to withstand higher applied accelerations and is safe from the perspectives of strength and rigidity.

Additionally, the Von Mises stress distribution and maximum shear stress distribution are examined and presented in Figure 10. The deformation contour is also investigated at the location of maximum deformation. From the Von-Mises stress analysis results, it is found that the maximum stresses are produced within the folded beam of the MEMS differential capacitive accelerometer. However, the magnitude of the maximum stresses produced within the proposed MEMS accelerometer is considerably lower than the material's yield limit. Moreover, the minimum Von Mises stresses are generated within the proof mass and at the anchor points. The regions with the highest stress value are presented in the zoomed view.

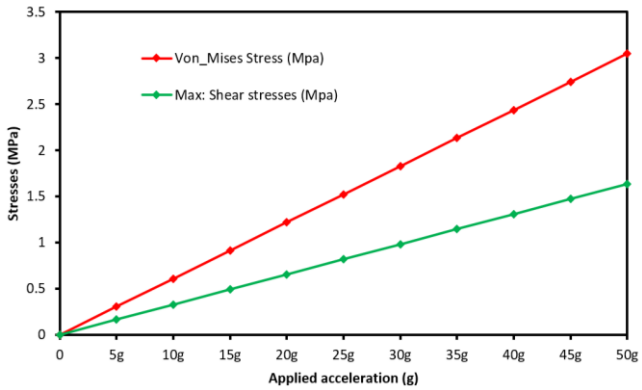

Figure 9. Stress distribution in the MEMS accelerometer at various applied acceleration magnitudes

3.3 Deflection and Mechanical Sensitivity Analysis

The variation of the deflection with the applied acceleration for the single-axis MEMS differential capacitive accelerometer is depicted graphically in Figure 10. A plot has been generated showing the MEMS accelerometer's deflection in its three principal axes (x, y, and z) versus applied accelerations spanning from -50g to +50g. The graph clearly indicates that the greatest deflection occurs along the axis, which is attributable to the acceleration being applied primarily in that same direction. Also, it can be observed from the graph that the deflection produced is in a linear relationship with the applied acceleration; thus, it is confirmed that the applied load is within the elastic limit and the

material follows Hook's law. On the other hand, the maximum deformation of approximately 181 nm is produced in the x-axis direction. In comparison, a relatively low deformation of about 0.0145 nm is produced in the y-axis direction, and approximately 1.03 nm deformation is produced in the z-axis direction. Besides, both theoretical methods and numerical simulations are employed to analyze the accelerometer's displacement sensitivity.

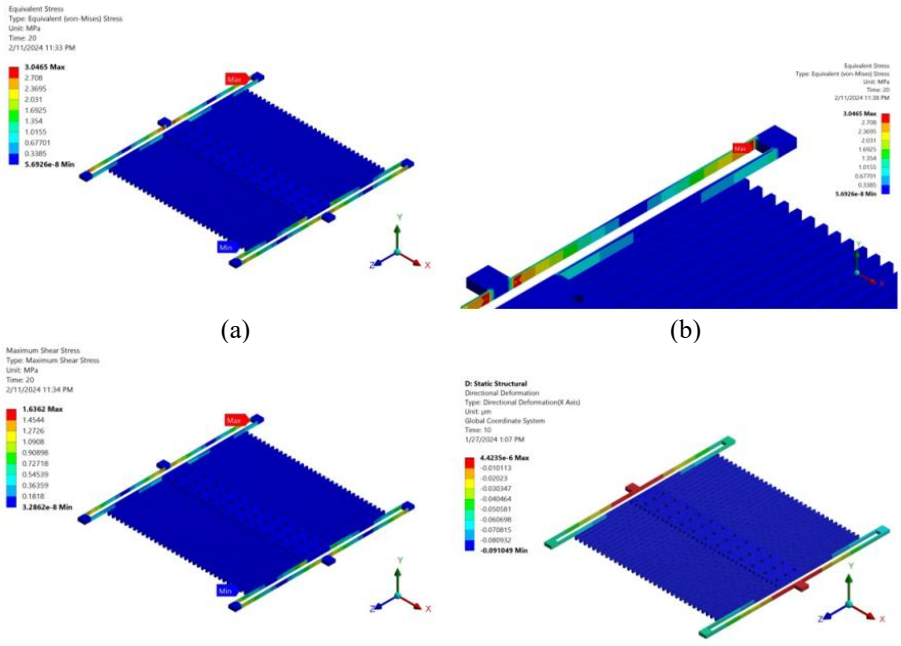

(a) (b) (c) (d)

Figure 10. Stress distribution over the MEMS accelerometer under applied acceleration (a) Von-Mises stresses (b) zoomed view of stress concentration region (c) Maximum Shear stress distribution (d) deformation of the accelerometer in the x-direction

The sensitivity's analytical value is determined via Equation (11). In contrast, the numerical value displacement sensitivity is quantified as the proof mass's displacement relative to each unit of applied acceleration, i.e, the slope of the displacement versus applied acceleration graph as presented in Figure 11. From the displacement versus applied acceleration graph, it can be observed that a significant deformation occurs along the x-axis, while a very small deformation is produced along the lateral axis. Moreover, the displacement sensitivity of the designed MEMS accelerometer, as computed using equation (11), is 3.27 nm/g, whereas the slope of the deformation graph against applied acceleration is 3.63 nm/g.

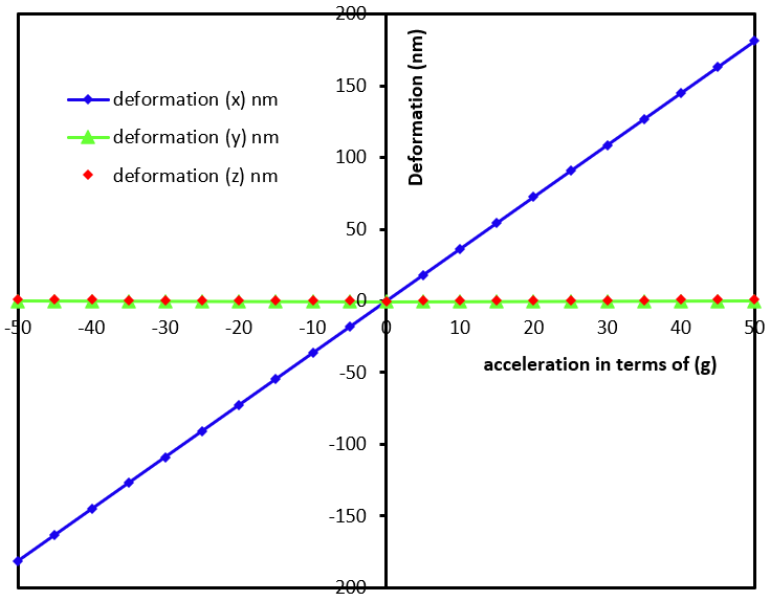

Figure 11. Displacement traveled by the proof mass of the single-axis MEMS accelerometer as a result of applied acceleration in the x-direction

3.4 Capacitive Sensitivity Analysis

The proposed single-axis differential MEMS accelerometer is, in fact, a capacitive accelerometer. This section of the study examines the capacitive sensitivity of the designed accelerometer, as illustrated in Figure 12. Similar to the displacement sensitivity, the term 'capacitive sensitivity' refers to the slope of the graphical representation showing capacitance alteration versus applied acceleration. This study, moreover, utilizes numerical simulation techniques to approximate the capacitive sensitivity of the designed accelerometer. The following equation is used to calculate the change in capacitance at various positions of the moving fingers.

$$\Delta C = 2C_0 \left[\frac{x}{d_0}\right] \tag{13}$$

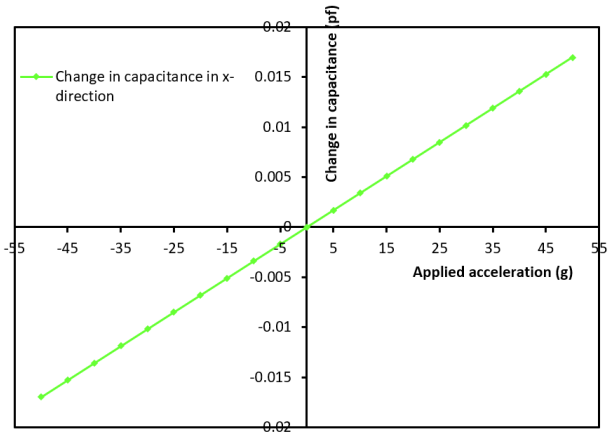

Figure 12. Applied Acceleration vs. Capacitance Change (pF)

According to Equation 13, C_0 represents the rest capacitance of the accelerometer at zero applied acceleration, d_0 signifies the capacitive gap, and x corresponds to the displacement resulting from the applied acceleration. The linear correlation between the applied acceleration and the change in capacitance is evident from the corresponding plot. Thus, the slope measured between any two points on this line reflects the capacitive sensitivity of the designed accelerometer, determined to be 0.000339 pF/g.

3.5 Analysis of Cross-Axis Effects in Accelerometers

The proposed accelerometer's performance characteristics are determined through a comprehensive analysis of multiple parameters, including its sensitivity, the upper limit of its operational range, nonlinearity, cross-axis sensitivity, and resolution capabilities. In this context, the present study introduces a compact and lightweight single-axis MEMS accelerometer for airbag application with an operating range of -50g to 50g. The displacement and capacitive sensitivity were presented and discussed. This subsection details the analysis and presentation of the cross-axis sensitivity for the designed accelerometer. Cross-axis sensitivity constitutes a crucial parameter in the performance analysis of a sensor. It is defined as the displacement produced in the sensing direction resulting from acceleration applied along an orthogonal axis [47]. The design objective for single-axis MEMS accelerometers is to accurately detect acceleration in a single, specific axis, concurrently providing substantial stiffness against movements in the other two perpendicular directions.

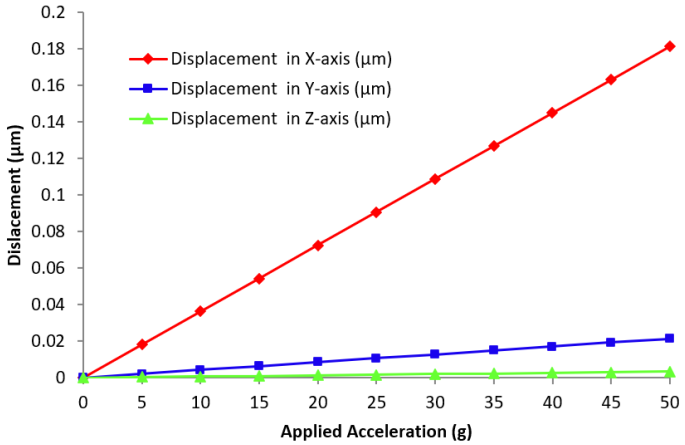

Figure 13. Cross-axis sensitivity performance of the proposed single-axis MEMS accelerometer under varying levels of applied acceleration (g)

The accelerometer's substantial stiffness in transverse directions ensures that any applied load induces only minimal displacement along these off-axis directions, leading to a negligible corresponding change in capacitance. To assess the cross-axis sensitivity of the designed accelerometer, Figure 13 plots the displacement in all three axes resulting from acceleration applied sequentially along each axis. As clearly illustrated by the graph, acceleration applied along the x-axis generates significant displacement. Conversely, when acceleration is applied along the y or z axes, the resulting displacements are very small, confirming the proposed accelerometer's high stiffness in directions orthogonal to its primary (x-axis) sensing direction.

3.6 Shock Test Analysis of the MEMS Capacitive Accelerometer

To ensure the safety of the passenger's automobile, a shock test using an accelerometer is carried out by explicit dynamics through the finite element method. To perform a shock test, a wall is positioned in front of the accelerometer, and the accelerometer is set to impact the wall at a velocity of 1×10^6 µm/s. Stresses and the deformation produced as a result of the shock were determined. The applied boundary conditions for the shock test analysis are presented in Figure 14 (a). Moreover, the deformation and stresses produced within the designed accelerometer were presented in Figure 14 (a) and (b). The stress analysis results showed that maximum stresses were produced within the folded beam near the anchors, with a value of approximately 294 MPa. Moreover, it was also found that the stress distribution within the accelerometer was highly nonlinear in nature, and the stresses produced were lower than the yield strength of the material. Thus, under this shock/impact velocity, the designed accelerometer will remain safe.

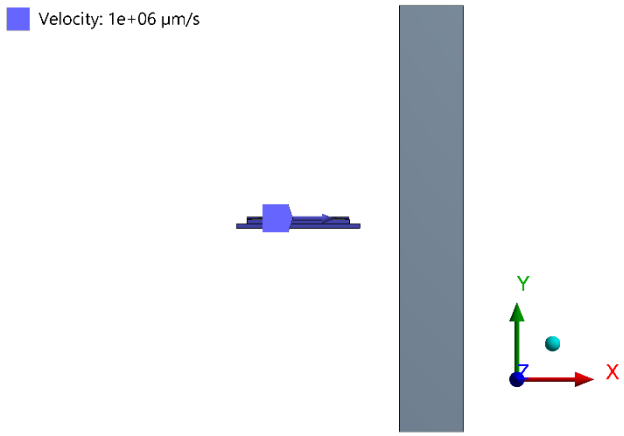

(a) Applied boundary conditions in shock test

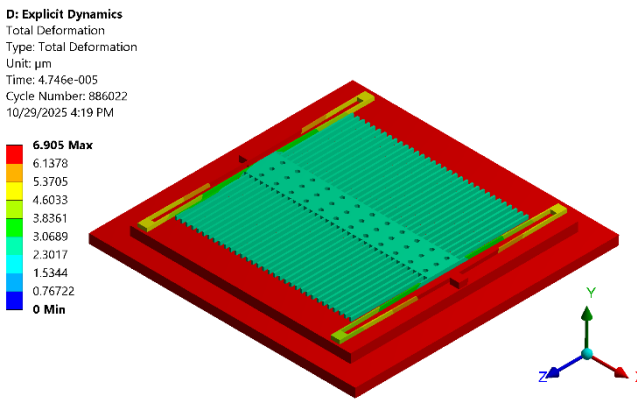

(b) Deformation produced as a result of impact

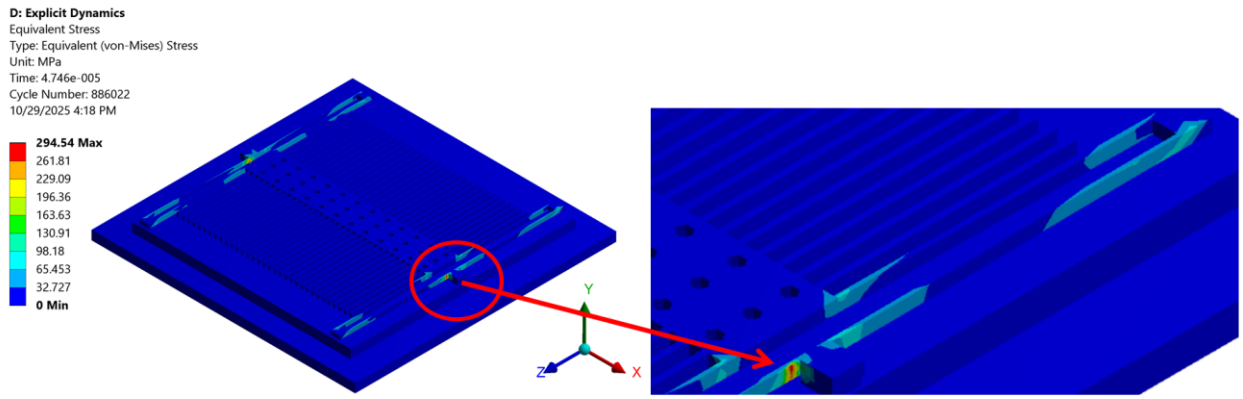

(c) Von-Mises stresses produced as a result of impact

Figure 14: Shock test analysis at the impact velocity of 1×10^6 µm/s (a) Applied boundary conditions in shock test (b) Deformation produced as a result of impact (c) Von-Mises stresses produced as a result of impact

3.7 Effect of Environmental Conditions on the Structural Performance of Accelerometer

To analyze the effect of environmental conditions, i.e., temperature, on the performance of the MEMS capacitive accelerometer, an initial thermal analysis was performed. Then, temperature variations within the accelerometer and heat flux were transferred to the mechanical model for thermal stress analysis. The designed accelerometer was tested under environmental conditions ranging from -50°C to 150 °C. The convection is applied to the upper side of the accelerometer with a film coefficient of 15 W/m^2 °C under natural convection conditions. The MEMS acclerometer models with applied boundary conditions and heat flux distribution are presented in Figure 15(a) and (b), respectively. Once the thermal analysis is completed, the thermal loads are transferred to ANSYS Mechanical for stress and deformation prediction as a

result of the applied environmental conditions. To determine stresses, the computational domain is discretised with a similar element type and element size as used for thermal analysis to achieve higher mapping of imported loads. Then the boundary conditions were applied to the MEMS acclerometer, where the acclerometer is fixed at both anchors to restrict thermal expansion. The governing equations were solved using the FE method, and then stresses and deformation were computed with the MEMS capacitive acclerometer. The poly-silicon material is used as a manufacturing material for the MEMS capacitive acclerometer. From the stress analysis results, it can be observed that maximum stresses are produced at the anchors due to the restriction of thermal expansion. Moreover, it was also observed that at approximately 150 °C, stresses of approximately 170 MPa were produced within the designed accelerometer. Additionally, the stresses produced within the designed accelerometer were lower than the yield strength of the material; thus, the designed accelerometer will remain safe from a structural point of view up to 150 °C.

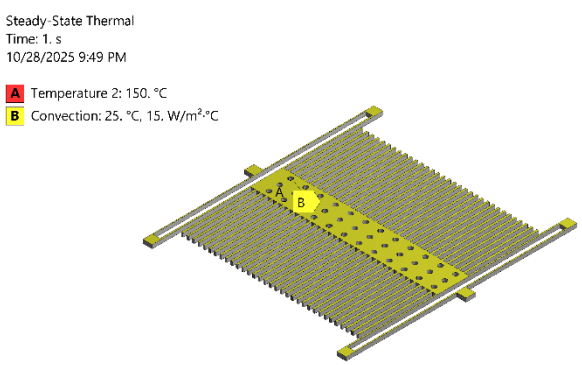

(a) Applied boundary conditions in thermal analysis

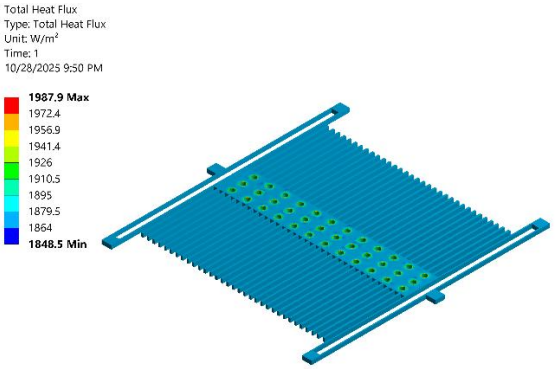

(b) Total heat flux

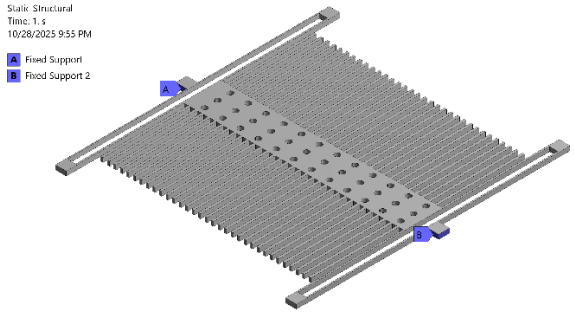

(c) Applied boundary conditions in thermal stress analysis

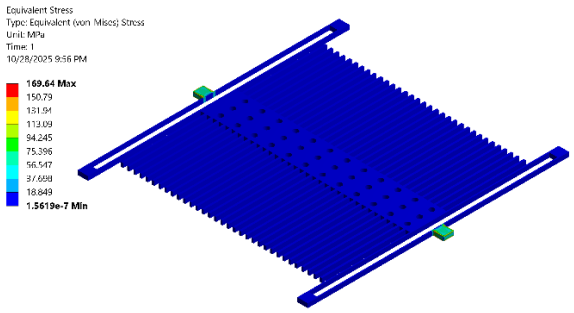

(d) Von-Mises stresses produced as a result of applied environmental conditions

Figure 15. Stresses produced due to environmental conditions, i.e., temperature (a) Applied boundary conditions in thermal analysis (b) Total heat flux (c) Applied boundary conditions in thermal stress analysis (d) Von-Mises stresses produced as a result of applied environmental conditions

Table 5. Comparison of the designed single-axis MEMS capacitive accelerometer with other reported MEMS accelerometers

Reference	Range (g)	Sensor area (mm^2)	Mass (µg)	Resonant frequency (Hz)	Mechanical sensitivity (nm/g)	Capacitive sensitivity (fF/g)
This work	±50	1	1.4	8332	3.63	0.339
[13]	12-75	2.72	----	1774	9.2	7
[52]	10	2.48	60.44	4270	13.9	80
[53]	10	1	32	2870	29.8	15.51
[54]	5	13.35	99	1500	121	225
[55]	5-10	4	59	4255	13.6	35
[56]	±8	16	60mg	100	----	-----

4. CONCLUSION

This study presents the design methodology and subsequent performance evaluation of a single-axis capacitive MEMS accelerometer. The accelerometer is designed for airbag applications, where the operating acceleration usually ranges from -50g to 50g. The accelerometer design parameters were selected after a detailed literature review to design a compact, lightweight, and highly sensitive single-axis MEMS accelerometer. The proposed compact MEMS capacitive accelerometer has a compact footprint of less than 1 mm × 1 mm and weighs about 1.4 µg. The accelerometer's weight is

reduced by introducing small holes in the proof mass; these etching holes help in the manufacturing process, allowing the proof mass to be released at the appropriate time.

Modal analysis indicates that the designed accelerometer exhibits a resonant frequency of approximately 8.3 kHz. When compared, the simulation and analytical results show a deviation of no more than 15%. To evaluate the structural integrity of the designed accelerometer, a stress analysis is conducted, revealing that the stresses produced for the applied envelope of acceleration values are substantially below the yield strength of the constituent material. The maximum σ_{VM} (Von-Mises stress) and τmax (maximum shear stress) experienced by the designed accelerometer are approximately 3.05 MPa and 1.64 MPa, respectively. The designed accelerometer has a mechanical sensitivity of 0.00363 μg and a capacitive sensitivity of approximately 0.000339 pF/g. Stress analysis results indicate that the proposed accelerometer can withstand accelerations between -100g and 100g without structural failure. Moreover, the study also tested a designed accelerometer under collision conditions, i.e., impact velocities of 1×10^6 μm/s, and the results found that the designed accelerometer remained safe under these conditions. The study also investigated the impact of surrounding temperatures on the performance and structural integrity of the designed accelerometer up to 150 °C. It was found that the designed accelerometer will remain safe under the aforementioned conditions.

Table 5 presents a comparison of the key performance parameters of the designed accelerometer with those of commercial and academic MEMS-capacitive accelerometers. From the table, it can be seen that the designed accelerometer is highly compact, lightweight, and capable of measuring acceleration over a wide range with comparable sensitivity. Another key advantage of the proposed MEMS-capacitive accelerometer is its simple design, holes over the proof mass significantly increase manufacturability and reduce the manufacturing cost of this miniature-sized device. In contrast, the recently reported literature on MEMS-capacitive accelerometers has a significantly large device area, weight, and a low acceleration measurement range. Moreover, the sensitivity of the proposed accelerometer is low; it may be enhanced in the future. Moreover, in future studies, fluid-structure interaction analysis will be used to understand the interaction between air and the device structure, enabling the precise prediction of the damping characteristics of air. Furthermore, optimization methods may be employed to optimize the performance of the MEMS-capacitive accelerometer.

ACKNOWLEDGEMENTS

No funding was allocated from the public, private, or not-for-profit sectors for this study.

CONFLICT OF INTEREST

All authors confirm the absence of any conflicts of interest regarding this work.

AUTHORS CONTRIBUTION

M. Al-Quran: Conceptualization, methodology, simulations, writing the draft manuscript and Visualization.

A. Al-Sheyyab: Simulations, Validation, reviewing and editing the manuscript, and project administration.

M. Al-Otain: Resources, literature review, and reviewing and editing the manuscript.

W. AlJaiuossi: Simulations, reviewing and editing the manuscript.

REFERENCES

[1] A. R. Chaudhuri, S. Severi, M. A. Erismis, L. A. Francis, and A. Witvrouw, "MEMS accelerometers combining a large bandwidth with a high capacitive sensitivity," *Procedia Engineering*, vol. 47, pp. 742-745, 2012.

[2] A. D'Alessandro, S. Scudero, and G. Vitale, "A review of the capacitive MEMS for seismology," *Sensors*, vol. 19, p. 3093, 2019.

[3] D. Xiao, Q. Li, Z. Hou, D. Xia, X. Xu, and X. Wu, "A double differential torsional micro-accelerometer based on V-shape beam," *Sensors and Actuators A: Physical*, vol. 258, pp. 182-192, 2017.

[4] G. Cosoli, S. Spinsante, and L. Scalise, "Wrist-worn and chest-strap wearable devices: Systematic review on accuracy and metrological characteristics," *Measurement*, vol. 159, p. 107789, 2020.

[5] M. Pollind, and R. Soangra, "Development and validation of wearable inertial sensor system for postural sway analysis," *Measurement*, vol. 165, p. 108101, 2020.

[6] S. Kavitha, R. Daniel, and K. Sumangala, "A simple analytical design approach based on computer aided analysis of bulk micromachined piezoresistive MEMS accelerometer for concrete SHM applications," *Measurement*, vol. 46, pp. 3372-3388, 2013.

[7] S. Kavitha, R. Daniel, and K. Sumangala, "Design and analysis of MEMS comb drive capacitive accelerometer for SHM and seismic applications," *Measurement*, vol. 93, pp. 327-339, 2016.

[8] Z. Mohammed, G. Dushaq, A. Chatterjee, and M. Rasras, "An optimization technique for performance improvement of gap-changeable MEMS accelerometers," *Mechatronics*, vol. 54, pp. 203-216, 2018.

[9] Z. Mohammed, I. Elfadel, and M. Rasras, "Monolithic multi degree of freedom (MDoF) capacitive MEMS accelerometers," *Micromachines*, vol. 9, p. 602, 2018.

[10] M. Benmessaoud, and M. Nasreddine, "Optimization of MEMS capacitive accelerometer," *Microsystem Technologies,* vol. 19, 2013, pp. 713-720.

[11] J. Weigold, K. Najafi, and S. Pang, "Design and fabrication of submicrometer single crystal Si accelerometer," *Journal of Microelectromechanical Systems*, vol. 10, pp. 518-524, 2001.

[12] J. Ramakrishnan, P. Gaurav, N. Chandar, and N. Sudharsan, "Structural design, analysis and DOE of MEMS-based capacitive accelerometer for automotive airbag application," *Microsystem Technologies*, vol. 27, pp. 763-777, 2021.

[13] R. A. Koochaksaraie, F. Barazandeh, and H. Barati, "A novel design of capacitive MEMS multi-range accelerometer; FEM and numerical approach," *Physica Scripta*, vol. 98, no. 11, p. 115026, 2023.

[14] A. Ivanov and A. Zhilenkov, "The use of IMU MEMS-sensors for designing of motion capture system for control of robotic objects," IEEE Conference of Russian Young Researchers in Electrical and Electronic Engineering (EIConRus), pp. 890-893, Moscow and St. Petersburg, Russia, 2018.

[15] J. Pansiot, Z. Zhang, B. Lo, and G. Yang, "WISDOM: wheelchair inertial sensors for displacement and orientation monitoring," *Measurement Science and Technology*, vol. 22, p. 105801, 2011.

[16] R. Rodr´ıguez-Mart´ın, C. P´erez-L´opez, A. Sam`a, J. Cabestany, and A. Catal`a, "A wearable inertial measurement unit for long-term monitoring in the dependency care area," *Sensor*s, vol. 13, pp. 14079-14104, 2013.

[17] S. Scudero, A. D'Alessandro, L. Greco, and G. Vitale, "MEMS technology in seismology: A short review," *IEEE International Conference on Environmental Engineering*, pp. 1-5, Milan, Italy, 2018.

[18] P. Ullah, V. Ragot, P. Zwahlen, and F. Rudolf, "A new high-performance sigma-delta MEMS accelerometer for inertial navigation," *DGON Inertial Sensors and Systems Symposium (ISS)*, pp. 1-13, Karlsruhe, Germany, 2015.

[19] S. Lu, S. Li, M. Habibi, and H. Safarpour, "Improving the thermoelectro-mechanical responses of MEMS resonant accelerometers via a novel multi-layer Perceptron Neural Network," *Measurement*, vol. 218, p. 113168, 2023.

[20] Y. Lei, et al. "Development of a high-precision and low cross-axis sensitivity 3-D accelerometer for low-frequency vibration measurement," *IEEE Sensors Journal*, vol. 23, no. 12, pp. 12634–12643, 2023.

[21] S. Ghasemi, B. Sotoudeh, and M. Pazhooh, "Design and simulation of a novel MEMS-based single proof mass three-axis piezo-capacitive accelerometer," *Microsystem Technologies*, vol. 30, no. 3, pp. 279–289, 2024.

[22] Z. Zhang, H. Zhang, Y. Hao, and H. Chang, "A review on MEMS silicon resonant accelerometers," *Journal of Microelectromechanical Systems*, pp. 1–35, 2024.

[23] M. Gupta, D. Bhatia, P. Kumar, M. Gupta, D. Bhatia, and P. Kumar, "Micro electrical mechanical system (MEMS) sensor technologies," in *Modern Intervention Tools for Rehabilitation*, Academic Press, 2023, pp. 25–44.

[24] S. Łuczak, M. Ekwińska, and D. Tomaszewski, "A method of precise auto-calibration in a micro-electro-mechanical system accelerometer," *Sensors*, vol. 24, no. 12, pp. 4018–4018, 2024.

[25] O. V. Oțăt, I. Dumitru, D Tutunea, L. Matei, and G. Marinescu, "Theoretical and experimental considerations regarding the airbag system operation," *IOP Conference Series Materials Science and Engineering*, vol. 1311, no. 1, pp. 012048–012048, 2024.

[26] Komalakumari, A. S, B. G N, C. J, and L. E, "Design of MEMS capacitive accelerometer for automotive airbag application," *International Journal of Advanced Research in Science, Communication and Technology*, vol. 8, no. 1, pp. 203–209, 2021.

[27] S. Veena, N. Rai, S. H. L, and V. S. Nagaraj, "Design and System Level Simulation of a MEMS Differential Capacitive Accelerometer," in *Emerging Research in Computing, Information, Communication and Applications*, S. N. R, P. L. M, and P. N. H, Eds. Singapore: Springer Nature Singapore, 2023, pp. 971–982.

[28] G. Sun, S. Chen, S. Zhou, J. Gan, and Y. Zhu, "Multi-objective optimization study of driver's airbag parameters," *Eighth International Conference on Electromechanical Control Technology and Transportation (ICECTT 2023)*, p. 55, 2023.

[29] A. Shrivastava, D. Behera, N. Reddy, and P. Aluru, *Optimization of Side Impact Airbag Design Using Response Surface Method*. No. 2023-01-0818. SAE Technical Paper, 2023.

[30] W. Liu, C. Yin, and G. Dou, "Design and Genetic Algorithm Optimization of a HighShockResistant MEMS Accelerometer Sensitive Structure for Automotive Airbag Applications," in *2025 26th International Conference on Electronic Packaging Technology (ICEPT)*, pp. 1–5.

[31] S. Wang, Y. Ma, W. Xu, Y. Liu, and F. Han, "Temperature compensation of MEMS resonant accelerometers with an on-chip platinum film thermometer," *Journal of Micromechanics and Microengineering*, vol. 33, no. 7, pp. 075004–075004, 2023.

[32] J. Zhang, T. Wu, Y. Liu, C. Lin, and Y. Su, "Thermal stress resistance for the structure of MEMS based silicon differential resonant accelerometer," *IEEE Sensors Journal*, vol. 23, no. 9, pp. 9146–9157, 2023.

[33] J. Liu and L. Piao, "Study on the sensitivity mechanism of low-coupled heat flow biaxial MEMS accelerometers," *IET Conference Proceedings*, vol. 2024, no. 9, pp. 220–224, 2025.

[34] T. Hongsakun, B. Tangtrakulwanich, N. Vittayaphadung, W. Thongruang, and S. Srewaradachpisal, "The effect of airbag design on impact attenuation for hip protection," *Engineering, Technology & Applied Science Research*, vol. 15, p. 4, 2025.

[35] T. Peng and Z. You, "Reliability of MEMS in Shock Environments: 2000–2020," *Micromachines*, vol. 12, no. 11, p. 1275, 2021.

[36] P. Vinay, C. Vamsi, M. Hemanth, A. Saiteja, M. A. Ali, and P. A. Kumar, "Design and simulation of MEMS based accelerometer for crash detection and air bags deployment in automobiles," *International Journal of Mechanical Engineering and Technology*, vol. 8, pp. 424–434, 2017.

[37] J. Zhang, Z. Yu, J. Yao, G. Yang, and Y. Su, "Investigating the mechanical behavior of antiimpact airbag fabrics: a structural design approach," *International Journal of Occupational Safety and Ergonomics*, pp. 1–13, 2025.

[38] J. Li, G. Lu, J. Liu, S. G. Niazi, and Y. Zeng, "Failure mechanism analysis and reliability assessment of MEMS accelerometers," *Quality and Reliability Engineering International*, vol. 41, no. 6, pp. 2547–2556, 2025.

[39] Z. Stanimirović and I. Stanimirović, "Advanced MEMS Technologies," *Microelectromechanical Systems (MEMS) - Innovation, Manufacturing Techniques and Applications*, p. 7, 2025.

[40] M. A. R. Tahir, M. M. Saleem, S. A. R. Bukhari, A. Hamza, and R. I. Shakoor, "An efficient design of dual-axis MEMS accelerometer considering microfabrication process limitations and operating environment variations," *Microelectronics International*, vol. 38, no. 4, pp. 144-156, 2021.

[41] M. Carratù, V. Gallo, P. Sommella, A. Pietrosanto, M. Catelani, L. Ciani, et al. "Development of a methodology for MEMS accelerometer health state estimation," *Proceedings of the XXIV IMEKO World Congress*, vol. 38, p. 101604, 2025.

[42] Y. Ma, X. Xu, and H. Li, "Optimization design of a capacitive microaccelerometer," *IEEE International Conference on Mechatronics and Automation*, Xi'an, China, pp. 1153-1157, 2010.

[43] O. Sidek, M. Afif, and M. Miskam, "Design and simulation of SOI-mEMS Z-axis capacitive accelerometer*," International Journal of Engineering and Technology*, vol. 10, p. 7, 2010.

[44] C. Sun, M. Tsai, Y. Liu, and W. Fang, "Implementation of a monolithic single proof-mass tri-axis accelerometer using CMOS-MEMS technique," *IEEE Transactions on Electron Devices*, vol. 57, pp. 1670-1679, 2010.

[45] W. Wai-Chi, A. Azid, and B. Majlis, "Formulation of stiffness constant and effective mass for a folded beam," *Archives of Mechanics*, vol. 62, pp. 405-418, 2010.

[46] G. Ananthasuresh, K. Vinoy, K. Bhat, S. Gopalakrishnan, and V. Aatre, Wiley–India, 2012.

[47] M. Bao, Micro mechanical transducers: pressure sensors, accelerometers and gyroscopes, (Elsevier, 2000).

[48] M. Benmessaoud and M. M. Nasreddine, "Optimization of MEMS capacitive accelerometer," *Microsystem Technologies*, vol. 19, no. 5, pp. 713–720, 2013.

[49] S. Chaterjee and G. Pohit, "Squeeze-Film Damping Characteristics of Cantilever Microresonators under Large Electrostatic Loading," *Mechanics of Advanced Materials and Structures*, vol. 19, no. 8, pp. 613–624, 2012.

[50] B. Chen and J. Miao, "Influence of deep RIE tolerances on comb-drive actuator performance," *Journal of Physics D Applied Physics*, vol. 40, no. 4, pp. 970–976, 2007.

[51] B. Vakili-Amini, "A Mixed-Signal Low-Noise Sigma-Delta Interface IC for integrated Sub-Micro-Gravity capacitive SOI accelerometers," 2006. [Online]. Available: https://smartech.gatech.edu/bitstream/1853/10437/1/amini_babak_v_200605-_phd.pdf

[52] R. Li, Z. Mohammed, M. Rasras, I. M. Elfadel, and D. Choi, "Design, modelling and characterization of comb drive MEMS gap-changeable differential capacitive accelerometer," *Measurement*, vol. 169, p. 108377, 2020.

[53] M. Keshavarzi and J. Y. Hasani, "Design and optimization of fully differential capacitive MEMS accelerometer based on surface micromachining," *Microsystem Technologies*, vol. 25, no. 4, pp. 1369–1377, 2018.

[54] R. Mukhiya, P. Agarwal, S. Badjatya, M. Garg, P. Gaikwad, S. Sinha, et al., "Design, modelling and system level simulations of DRIE-based MEMS differential capacitive accelerometer," *Microsystem Technologies*, vol. 25, no. 9, pp. 3521–3532, 2019.

[55] Z. Mohammed, G. Dushaq, A. Chatterjee, and M. Rasras, "An optimization technique for performance improvement of gap-changeable MEMS accelerometers," *Mechatronics*, vol. 54, pp. 203–216, 2017.

[56] STMicroelectronics, "AIS328DQ: 3-Axis ±2g/±4g/±8g Digital Output Low-Power High-Performance Accelerometer," Datasheet, 2025. [Online]. Available: https://www.st.com/resource/en/datasheet/ais328dq.pdf